To be published in Optics Letters:

Title: Near-UV optical cavities in Ga2O3 nanowires

Authors: Manuel Alonso-Orts,Gerwin Chilla,Rudolfo Hötzel,Emilio Nogales,José M San Juan,María L Nó,Martin Eickhoff,Bianchi Méndez

Accepted: 01 December 20

Posted 02 December 20

DOI: https://doi.org/10.1364/OL.410757

Near-UV optical cavities in Ga_2O_3 nanowires

Manuel Alonso-Orts,[1,2,*] Gerwin Chilla,[2] Rudolfo Hötzel,[2], Emilio Nogales,[1] José M. San Juan,[3] María L. Nó,[4] Martin Eickhoff,[2] and Bianchi Méndez[1]

[1] *Departamento de Física de Materiales, Plaza Ciencias 1, Universidad Complutense de Madrid, 28040, Madrid, Spain*
[2] *Institute of Solid State Physics, University of Bremen, Otto-Hahn-Allee 1, 28359, Bremen, Germany*
[3] *Departamento de Física de la Materia Condensada, Facultad de Ciencias y Tecnología, Universidad del País Vasco, Apdo. 644, 48080 Bilbao, Spain*
[4] *Departamento de Física Aplicada II, Facultad de Ciencia y Tecnología, Universidad del País Vasco, Apdo. 644, 48080 Bilbao, Spain*

**Corresponding author: man.alonso.orts@gmail.com*

Received XX Month XXXX; revised XX Month, XXXX; accepted XX Month XXXX; posted XX Month XXXX (Doc. ID XXXXX); published XX Month XXXX

In this letter, we report optical confinement in the near-UV range in Ga_2O_3 nanowires by distributed Bragg reflector (DBR) nanopatterned cavities. High-contrast DBRs, which act as the end mirrors of the cavities of the desired length, are designed and fabricated by Focused Ion Beam (FIB) etching. The resonant modes of the cavities are analyzed by micro-photoluminescence measurements, analytical models and simulations, which show very good agreement between each other. Experimental reflectivities up to 50% are obtained over the 350-410 nm region for the resonances in this wavelength range. Therefore, Ga_2O_3 nanowire optical cavities are shown as good candidates for single-material-based near-ultraviolet (near-UV) light emitters.

Near-UV light emitters are required for applications such as solid-state lightning (SSL), communications, optical sensing or security features, among others [1-3]. So far, InGaN and AlGaN materials have been mainly used for these purposes and remarkable progress has been made, but the current devices exhibit low external quantum efficiencies at wavelengths below 365 nm [1]. Among the alternative near-UV emitting materials, β-Ga_2O_3 is of high interest. The material's low cost and high thermal stability, along with its high electric breakdown field, have made Ga_2O_3 worth of remarkable attention in the last years [4, 5]. Its ultra-wide band gap (4.8 eV) results in a wide transparency range and an intrinsic luminescence in the UV-blue range (2.8-3.6 eV) at room temperature [4, 6]. Until recently, the optical applications of Ga_2O_3 have mostly pivoted around the solar-blind photodetector market [7].

A reduction in the operational wavelength is desirable to develop small size, high-density stable photonic devices. These devices should require nanostructures as building blocks which are capable of withstanding high optical powers in order to achieve good performance. In this sense, the potential applications in high power optics of Ga_2O_3 in the nanoscale have recently been demonstrated [8]. Therefore, it is interesting to further explore the use of Ga_2O_3 in nanophotonic applications, in particular in short-wavelength devices, owing to its intrinsic luminescence in this range.

In this work, near-UV optical cavities based on unintentionally doped (UID) Ga_2O_3 have been designed, fabricated and analyzed. The optical cavities have been realized by patterning distributed Bragg reflector (DBR) mirrors in the UID nanowires by Focused Ion Beam (FIB). This approach has recently been applied in Cr doped Ga_2O_3 optical microcavities in the red-NIR wavelength range (680 – 750 nm), in which the tunability in their resonant wavelengths was accomplished by means of a rational design of the DBR pattern [9, 10]. As UID Ga_2O_3 usually exhibits rather strong luminescence in shorter wavelength ranges (350 – 410 nm), we have made use of these techniques in order to obtain near-UV range optical nanocavities of Ga_2O_3 in the present work.

UID Ga_2O_3 nanostructures were synthesized in a single-step treatment at 900ºC during 6 hours under Ar flow of 0.8 l/min. A gallium oxide pellet was used as substrate and a metallic gallium bit was placed on top of the substrate as the source material. The furnace was not sealed for vacuum, which allowed for the oxidation of the metallic Ga. During the thermal treatment, long and taper-free Ga_2O_3 micro- and nanowires (NWs) were formed on top of the pellet via the vapor-solid mechanism, similarly to previous works [11]. The micro-Raman spectra of these NWs, obtained in a confocal microscope by excitation with a He-Cd laser (325 nm), show the characteristic peaks of the monoclinic (β phase) of Ga_2O_3 (Fig. S1). By approximating with tweezers a bundle of the NWs from the pellet to the TEM grid, individual almost free-standing NWs were prepared for optical analysis, which avoided eventual optical losses from any contact between the NWs and the substrate [12]. To build the DBRs, predefined sets of periodic holes were carved in some

selected NWs in a Focused Ion Beam (FIB) instrument (Helios 650) at 30 kV and 8 pA. Secondary Electron (SE) images of the structures were obtained in the FEI Helios 650 or the FEI Nova Nanolab 200. Micro-photoluminescence (μ-PL) characterization was performed in a custom-made setup (Horiba) confocal microscope by exciting with a Magellan diode-pumped Yb-doped fiber oscillator laser (Clark-MXR Inc.) with E = 4.8 eV (λ = 257 nm). An ultra-broadband wire grid linear polarizer was used for polarized μ-PL measurements.

Fig. 1(a) shows the general design of the DBR cavity. It is formed by patterning a set number (N) of periodic rectangular holes in the nanowire, thus defining an active region of length L between them. It should be noticed that the optical length of the cavity, which determines the Free Spectral Range (FSR) between two adjacent resonant peaks, can be selected in this fabrication procedure by carving the DBRs at the desired distance from each other. Fig. 1(b) is an SE image of a fabricated Ga_2O_3 DBR cavity (cavity 1) with N = 15 and L_1 =12.0 μm. Fig. 1(c) is a higher magnification SE image of three periods of one of its DBRs. From these images, the dimensions of the NW and the DBRs were obtained.

Fig. 1(d) shows a different nanopatterned cavity (cavity 2) with a length of L_2 = 12.4 μm and N=15 periods. Table 1 presents a comparison of the parameters of both cavities, as measured from SE images. As shown in this table, both NWs do not have rectangular cross-sections. Rather, it is an irregular hexagon, with $a_t < a$, where a_t is the NW's top facet while a is the total width of the NW (see Fig. S2). The DBRs in both cavities have been designed with the same periodicity (Λ = 280 nm), while there are slight variations in the NW and DBR hole dimensions.

Table 1. Parameters of the DBR cavities

DBR cavity	a (nm)	a_t (nm)	b (nm)	L (μm)	α (nm)	γ (nm)
Cavity 1	500	220	640	12.0	130	200
Cavity 2	500	380	460	12.4	150	290

a = NW width, a_t = NW top facet, b = NW depth, L = cavity length, α = DBR hole length, γ = DBR hole width. Both DBRs have the same periodicity: Λ = 280 nm.

Figs. 2(a) and 2(b) show μ-PL spectra from cavities 1 and 2, respectively. They were obtained at the confocal microscope by the use of a custom design module analogous to [13], which allows to locate the excitation laser spot (~3 μm spatial FWHM, objective NA = 0.5) at the active region and the collection point at one of the DBRs, where the guided light is partially scattered (see inset in Fig. 2(b)). As expected [6], the luminescence of the Ga_2O_3 NWs is in the near-UV range. In cavity 1, Fig. 2(b), weak resonances appear in the unpolarised spectrum (Fig. S3), which are enhanced by placing the polarizer perpendicular to the NW axis. The axes are defined as follows: z is parallel to the NW length while x is perpendicular to the NW length and the optical axis, y [9]. The highest intensity and finest peaks of cavity 1 appear around 400 nm. In cavity 2, Fig. 2(b), very intense resonances are observed in the 370-400 nm range already without the need of a polarizer, and further well-resolved resonances appear for λ < 360 nm. It should be noted that μ-PL spectra collected on unpatterned NWs (i.e. NWs without DBRs) of the same sample did not show any resonances (Fig. S4).

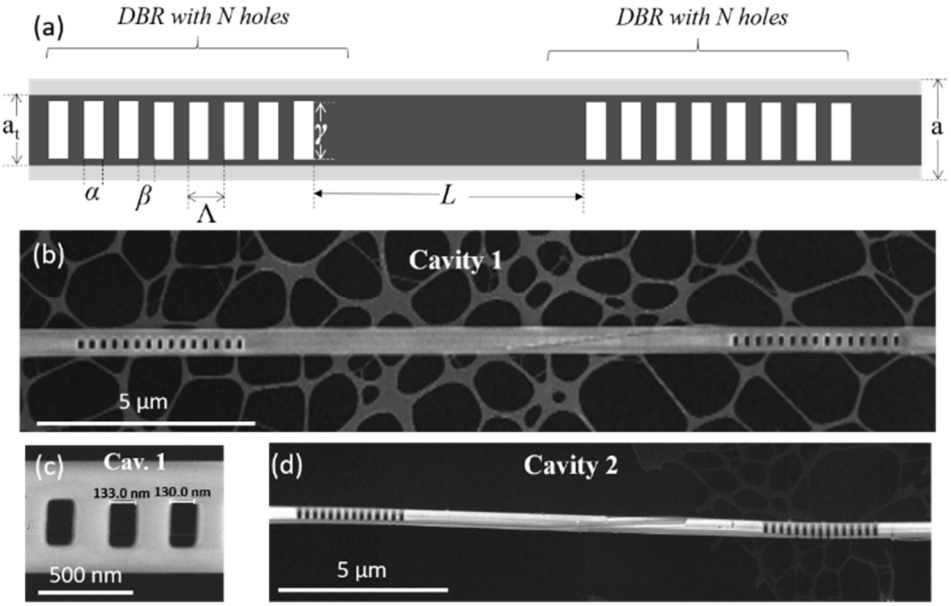

Fig. 1. (a) Schematic of the parameters of the DBR cavity. (b) SE image of cavity 1. (c) Higher magnification image of a DBR of cavity 1, showing 3 periods. (d) SE image of cavity 2.

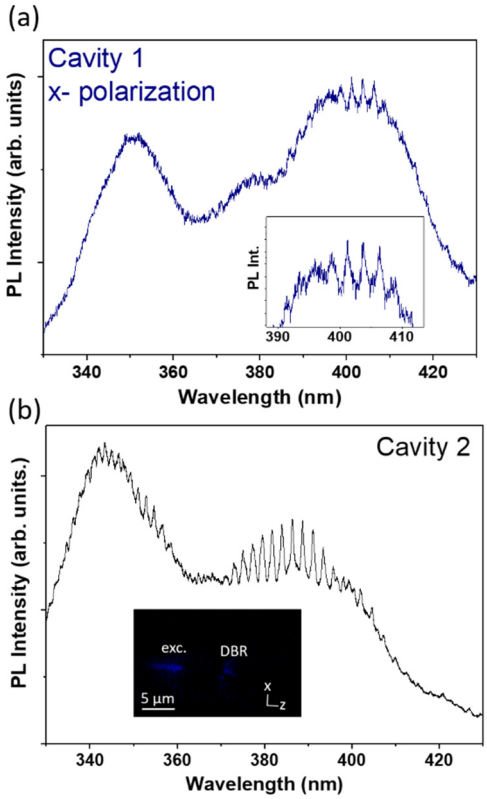

Fig. 2. (a) µ-PL spectrum from DBR cavity 1, obtained with the polarizer placed parallel to the x-axis. The inset shows a magnified view of the resonances. (b) µ-PL spectrum from DBR cavity 2, recorded without a polarizer. The inset is an optical microscope image of the µ-PL emission of cavity 2, indicating the excitation point and the position of the DBR.

From the wavelength position of the resonances, the effective length (L_{eff}) of the cavity can be obtained by using the longitudinal Fabry-Pérot resonance condition [Eq. (1)]:

$$L_{eff} = l\frac{\pi}{k_z} \qquad (1)$$

Here, l is an integer and k_z represents the value of the wavevector component parallel to the wire axis. If k_z is known for each peak, the longitudinal resonance condition [Eq. (1)] can be applied for each of the resonant peaks. However, to obtain the k_z values, methods such as the analytical Marcatili expressions for dielectric rectangular waveguides [9, 14] must be employed. The validity of the Marcatili method for the present type of NWs was discussed in ref. [9]. Considering that the cross-sectional shape of cavity 2 is closer to a rectangle than that of cavity 1 we applied this method for the former. Consecutive l values were obtained for consecutive resonant peaks, and the value of L_{eff} = 13.3 µm was obtained for cavity 2. This length exceeds the physical length (L) between both DBRs by 0.9 µm, which is attributed to the penetration depth of the resonant modes in the DBRs [15]. In the case of cavity 1, similar FSRs were obtained at 399-406 nm, which fits with the similar L of both DBR cavities.

The reflectivity of the DBRs that form the cavities can be extracted experimentally from the finesse (F) value of the resonant peaks. This parameter provides a useful indicator for the quality of the optical resonances in terms of optical losses. It is obtained from the division of the FSR between one resonant peak and its adjacent one ($\Delta\nu$) and the peak's full width half maximum (FWHM, $\delta\nu$) [Eq. (2)]:

$$F = \frac{\Delta\nu}{\delta\nu} \simeq \frac{\Delta\lambda}{\delta\lambda} \qquad (2)$$

An example of the experimental finesse calculation from experimental µ-PL results is shown in Fig. 3(a), which displays a magnification of the spectrum in Fig. 2(b) (cavity 2), showing the resonances at 386.3 nm, 388.7 nm and 391.0 nm. The F values of the cavities range from 2.9 to 4.4. From these results, assuming that both DBRs have the same reflectivity (R), [Eq. (3)] was used to calculate the experimental value for R [16]:

$$F = \frac{\pi\sqrt{R}}{1-R} \qquad (3)$$

As R depends on the incident wavelength, F and R values vary throughout the emission range. Moderate R values were obtained for the DBRs, ranging from 38% to 44% in cavity 1 and from 41% to 49% in cavity 2. These values are notably higher than the expected reflectivity of Ga_2O_3 wires due to refractive index difference between the NW end and the surrounding air, which is around 10% for normal incidence [9]. Therefore, the patterned DBRs in both cavities indeed act as partial reflecting mirrors, with an improved reflectivity over the wire ends in the selected wavelength ranges.

To further assess the optical properties of both DBR cavities, simulations with the commercial OptiFDTD software were carried out. The experimentally determined dimensions, the dispersive refractive index of β-Ga_2O_3 [17] and the actual cross-section of each NW, as well as the SEM parameters of the 15-hole FIB-etched DBR were implemented in each of the two simulations. Fig. 3(b) shows the design for the FDTD simulation for cavity 2. A Gaussian modulated continuous wave centered at 370 nm wavelength was set to propagate just before the DBR. Two detection planes were placed before and after the DBR in order to obtain the reflected and transmitted power, respectively. The reflection and transmission spectra for DBR cavities 1 and 2 are shown in Figs. 3(c) and 3(d) in lines colored blue or black (reflection, respectively) and red (transmission). The experimental R results are included in the graphs in purple. It must be noted that test simulations were also performed taking into account possible variations of the refractive index due to anisotropy [18] and showed almost identical results.

In cavity 1, the simulated reflectivity maximum in the emission range for x-polarization (blue line) is R = 45%, which matches with the highest experimental reflectivity. However, the simulated R_{max} is located around 413-414 nm, which seems to be slightly red-shifted, about 10 nm, with respect to the highest R experimental peak, as indicated in Fig. 3(c). This difference, along with the lower quality of the experimental resonances in the rest of the emission range of this cavity, might be due to structural defects in the cavity or to possible differences between the real cross-section of the wire and the modelled one.

In cavity 2 (Fig. 3(d)), very good agreement is found between the simulated and the experimental results. In this case, both show higher reflectivities with respect to cavity 1 in the whole emission range, reaching values up to almost 50% in several wavelength intervals, from the near-UV (~350 nm) to the violet (~400 nm). Both the simulations and the experimental results indicate the possibility of tuning the highest reflectivity range by modifying the NW dimensions or the DBR parameters.

The results also show room for improvement. In cavity 2, the simulated transmission (T) of the DBRs is lower than 10% while R, both simulated and experimental, is at best around 50%. Therefore, as $R + T + S = 1$, more than 40% of the power is expected to be lost due to scattering (S) at the DBRs. Therefore, alternative DBR designs such as higher number of incompletely milled holes [19] or tapered designs [20] would be necessary in order to reduce the scattering at the DBRs and further improve the optical quality and the tunability of the Ga_2O_3 UV-emitting DBR nanopatterned cavities.

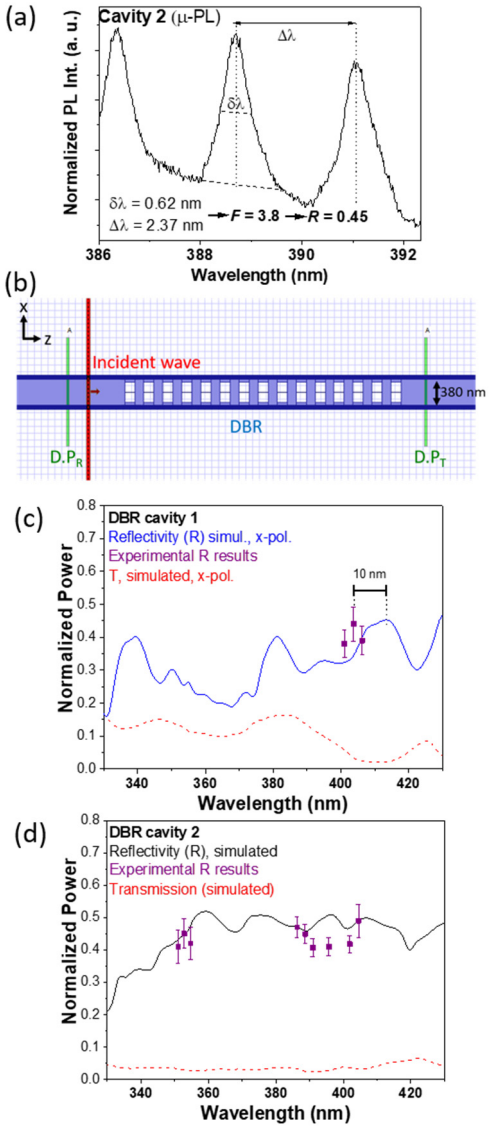

Fig. 3. (a) Experimental finesse (F) and reflectivity (R) results from the 389 nm μ-PL peak in cavity 2. (b) Top view of the FDTD-designed cavity 2. An incident Gaussian modulated continuous wave (in red) was placed just before the DBR and detection planes, $D.P_R$ and $D.P_T$, were placed before and after the DBR, respectively. A similar design was made for cavity 1. (c) Comparison of the FDTD-simulated reflected power spectrum in x-polarization (blue) and experimental R results (purple) for cavity 1. (d) Comparison of the FDTD-simulated reflected power spectrum (black) and the experimental R results (purple). Simulated transmitted (T) power through the DBR is shown in dashed red.

In summary, we have achieved the design, fabrication and characterization of Ga_2O_3 optical cavities in the near-UV range (350 -410 nm) with rather good performance by virtue of suitable DBR patterning. Experimental μ-PL resonant modes have been obtained on two FIB-fabricated nanopatterned cavities due to reflection at the limiting DBRs, as confirmed by analytical calculations. Very good agreement of the experimental and the simulated performance of the cavities has been observed, with reflectivities ranging from 38% to 50% in the emission range of the NWs. The results pave the way for highly stable well-defined Ga_2O_3 UV photonic devices in the micro- and nanoscale.

Funding sources
Placeholder for funding.

Acknowledgments. This work has been supported by MINECO projects M-ERA.NET PCIN-2017-106 and RTI2018-097195-B-I00. M. A-O acknowledges financial support from MICINN (FPU contract No. FPU15/01982), including finance for his short stay at Bremen University. This work made use of the FIB facilities from the SGIKER of the UPV/EHU. The authors also thank the Air Force Office of Scientific Research (Grant: FA8655-20-1-7013).

Disclosures
The authors declare no conflict of interest.
See Supplement 1 for supporting content.

References

1. M. Kneissl, T. Y. Seong, J. Han, and H. Amano, Nature Photonics **13**, 233-244 (2019).
2. Z. Y. Xu, and B. M. Sadler, Ieee Communications Magazine **46**, 67-73 (2008).
3. A. K. Singh, S. Singh, and B. K. Gupta, Acs Applied Materials & Interfaces **10**, 44570-44575 (2018).
4. Z. Galazka, Semiconductor Science and Technology **33**, 113001 (2018).
5. S. J. Pearton, J. C. Yang, P. H. Cary, F. Ren, J. Kim, M. J. Tadjer, and M. A. Mastro, Applied Physics Reviews **5**, 56 (2018).
6. T. Onuma, Y. Nakata, K. Sasaki, T. Masui, T. Yamaguchi, T. Honda, A. Kuramata, S. Yamakoshi, and M. Higashiwaki, Journal of Applied Physics **124**, 075103 (2018).
7. J. J. Xu, W. Zheng, and F. Huang, Journal of Materials Chemistry C **7**, 8753-8770 (2019).
8. H. Y. Deng, K. J. Leedle, Y. Miao, D. S. Black, K. E. Urbanek, J. McNeur, M. Kozak, A. Ceballos, P. Hommelhoff, O. Solgaard, R. L. Byer, and J. S. Harris, Advanced Optical Materials **8**, 1901522 (2020).
9. M. Alonso-Orts, E. Nogales, J. M. San Juan, M. L. No, J. Piqueras, and B. Mendez, Physical Review Applied **9**, 064004 (2018).
10. M. Alonso-Orts, E. Nogales, J. M. San Juan, M. L. No, and B. Mendez, SPIE Proceedings **10919**, 10919S (2019).
11. M. Alonso-Orts, A. M. Sanchez, S. A. Hindmarsh, I. Lopez, E. Nogales, J. Piqueras, and B. Mendez, Nano Letters **17**, 515-522 (2017).
12. E. Nogales, B. Mendez, and J. Piqueras, Ultramicroscopy **111**, 1037-1042 (2011).
13. R. M. Ma, X. L. Wei, L. Dai, S. F. Liu, T. Chen, S. Yue, Z. Li, Q. Chen, and G. G. Qin, Nano Letters **9**, 2697-2703 (2009).
14. E. A. Marcatili, Bell System Technical Journal **48**, 2071-+ (1969).
15. L. R. Brovelli, and U. Keller, Optics Communications **116**, 343-350 (1995).
16. M. Suter, and P. Dietiker, Applied Optics **53**, 7004-7010 (2014).
17. M. F. Al-Kuhaili, S. M. A. Durrani, and E. E. Khawaja, Applied Physics Letters **83**, 4533-4535 (2003).
18. C. Sturm, R. Schmidt-Grund, C. Kranert, J. Furthmuller, F. Bechstedt, and M. Grundmann, Physical Review B **94**, 035148 (2016).
19. A. Fu, H. W. Gao, P. Petrov, and P. D. Yang, Nano Letters **15**, 6909-6913 (2015).
20. A. R. M. Zain, N. P. Johnson, M. Sorel, and R. M. De la Rue, Optics Express **16**, 12084-12089 (2008).